ISSN: 0067-2904

Theoretical and Experimental Studies for Inhibition Potentials of Imidazolidine 4-One and Oxazolidine 5-One Derivatives for the Corrosion of Carbon Steel in Sea Water

Rehab M. Kubba*, Nada M. Al-Joborry, Naeemah J. Al-lami
Department of Chemistry, College of Science, University of Baghdad, Baghdad, Iraq

Received: 9/10/2019 Accepted: 21/1/2020

Abstract

Two derivatives of Iimidazolidin 4-one (IMID4) and Oxazolidin 5-one (OXAZ5), were investigated as corrosion inhibitors of corrosion carbon steel in sea water by employing the theoretical and experimental methods. The results revealed that they inhibit the corrosion process and their %IE followed the order: IMID4 (89.093%) > OXAZ5 (80.179%). The %IE obtained via theoretical and experimental methods were in a good agreement with each other. The thermodynamic parameters obtained by potentiometric polarization measurements have supported a physical adsorption mechanism which followed Langmuir adsorption isotherm. Quantum mechanical method of Density Functional Theory (DFT) of B3LYP with a level of 6-311++G (2d, 2p) were used to calculate the geometrical structure, physical properties and inhibition efficiency parameters, in vacuum and two solvents (DMSO and H_2O), all calculated at the equilibrium geometry, and correlated with the experimental %IE. The local reactivity has been studied through Mulliken charges population analysis. The morphology of the surface changes of carbon steel were studied using SEM and AFM techniques.

Keywords: Imidazolidine, Oxazolidine, Corrosion inhibitors, Quantum chemical calculations, Thermodynamic parameters.

الدراسات النظرية والتجريبية على إمكانات المشتقين إيميدا زولدين 4-اون وأوكسازوليدين 5-اون لتثبيط تآكل حديد الصلب الكربوني في مياه البحر

رحاب ماجد كبة*، ندي محمد الجبوري، نعيمة جبار اللامي
قسم الكيمياء كلية بغداد، جامعة بغداد، بغداد، العراق

الخلاصه

تم التحقق من قابلية المشتقين إيميدازولدين 4-اون (IMID4) و أوكسازوليدين-5-اون (OXAZ5)، كمثبطي تآكل لسطح حديد الصلب الكربوني في ماء البحر باستخدام الطرق النظرية والتجريبية. بينت النتائج عن أنهما يمنعان التآكل بكفاءة تثبيط تتبع الترتيب (80.179%) OXAZ5 < (89.093%) IMID4. تم الحصول عى هذه الكفاءة من الطرق النظرية والتجريبية اللتين تطابقت نتائجهما بشكل جيد. دعمت المعلمات الديناميكية الحرارية التي تم الحصول عليها باستخدام قياسات استقطاب الجهد آلية الامتزاز الفيزيائي وتبعت امتزاز لنكماير. وقد تم استخدام طريقة حسابات ميكانيك الكم وفق نظرية دوال الكثافة (DFT) عند المستوى (2d,2p) 6-311++G (B3LYP)) لحساب التركيب الهندسي والخصائص الفيزيائية ومعايير كفاءة

*Email: Rehab_mmr_kb@yahoo.com

التثبيط في الفراغ وفي المذيبين DMSO و H_2O. وقد تم حسابها جميعا عند الشكل الهندسي التوازني. وتمت دراسة تمركز المواقع الفعالة من خلال تحليل موليكان للشحنات. وتمت دراسة مورفولوجيا التغيرات السطحية للفولاذ الكربوني باستخدام تقنيات الفحص المجهري للإلكترون (SEM) و الفحص المجهري للقوة الذرية (AFM).

1. Introduction

Corrosion of metals is a serious material deterioration problem from both structural and economic integrity standpoint, but it can be largely controlled by the suitable strategies. Carbon steel (C.S) is being widely used as engineering alloy, however, corrosion of carbon steel occurs in almost all practical environments [1]. Metallic corrosion is a spontaneous process ($\Delta G < 0$) that causes damage in almost all sections of human activity. Among the most influenced structures are the pipes for oil transportation [2]. The biggest anxiety of the corrosion scientists is efficient protection of the metals without disturbing the environmental peace. Hence, the study of corrosion processes and their inhibition turn out to be the main goal of many researchers now [3]. Basically, corrosion inhibitor is a substance added in a small amount of the corrosive environment to reduce the corrosion rate of the metal or alloys [4]. Most inhibitors utilized in manufacturing are organic compounds. These organic inhibitors containing donor atoms such as O, S and N. Inhibitors including triple or double bonds had an important role in simplifying the adsorption process of these compounds [5]. The type of mechanism that inhibitors applied was adsorption mechanism, these mechanism summarized in adhere the inhibitor molecule on the metal surface to form a protective barrier against corrosive agents in the environment. The adsorbed molecule of inhibitors can affect the corrosion reaction either by physically blocking the active sites presents on the metal surface, or by changing the activation barriers of the anodic and cathodic partial reactions of the corrosion process, or may be both [6]. The study of inhibition efficiency also involved quantum calculations to support the experimental results. In density function theory (DFT) the researcher has to test huge number of organic compounds to select a potential corrosion inhibitor. This type of search costs money, effort and time. However, the development of hardware and software technology in this field makes it capable to choose a good corrosion inhibitor from organic compounds with reduced cost, effort and time [7].

The aim of this work is to study the inhibition efficiency of two organic compounds of (IMID4) and (OXAZ5) [8], see Figure-1. The inhibition of (IMID4) and (OXAZ5) were studied experimentally in saline solution of 3.5% NaCl using potentiostatic polarization meaurements, and theoretically, using DFT method of (6-311/ B3LYP++G (2d, 2p)) level using Gaussian 09 program. These calculations were done for obtaining the parameters of the corrosion efficiency in three media (vacuum, DMSO, and water). (IMID4 and OXAZ5 were also recently proved to have a wide range of biological and pharmacological activities, anti-tumor and anti oxidant activities [8]).

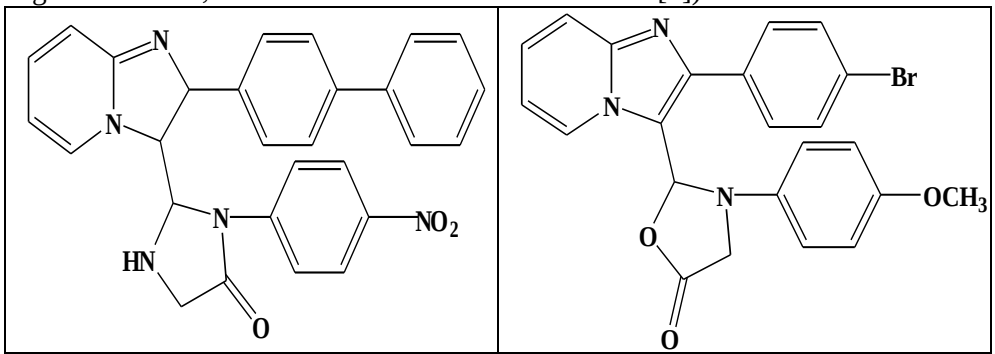

Figure 1-Two dimensions chemical structures of the studied organic inhibition compound for the corrosion of carbon steel in sea waters; 2-(2-biphenyl-4-yl-2,3- dihydro-imidazo [1,2-a] pyridine-3-yl)-3-(4-nitro-phenyl)-imidazolidin-4-one (IMID4) and 2-[2-(4-bromo-phenyl)-imidazo [1,2-a] pyridine-3-yl]-3- (4-methoxy-phenyl)-oxazolidin-5-one (OXAZ5).

2. Experimental details

2.1. Preparation of carbon steel samples

Carbon steel's rod was symbolized as (C45) with the following percentage of metallic materials in composition (wt %): (0.122% C, 0.206% Si, 0.641% Mn, 0.016% P, 0.031% S, 0.118% Cr, 0.02% Mo, 0.105% Ni, and 0.451% Cu) [9]. The rod mechanically cutting into pieces forming a cyclic specimen of carbon steel with 1.6 cm diameter and 3 mm thickness, each of these specimen was refined with emery paper (silicon carbide SiC) in different grades (80, 150, 220, 320, 400, 1000, 1200 and 2000) grades, then washed with tap water, distilled water and degreased with acetone, washed again with distilled water, and finally held in a desiccators after it is dried in room temperature.

2.2. Preparation of solutions

2.2.1. Salt blank solution

35 gm of sodium chloride (NaCl) was dissolved in (100 ml) distilled water; then transferred into 1liter volumetric flask which contained 6ml of dimethyl sulfoxide (DMSO) solvent. The solution volume was then completed to (1L) with distilled water. We used 3.5% NaCl in this study in order to avoid some problems related to ohmic drop.

2.2.2. Preparation of salty solutions of 2-(2-Biphenyl-4-yl-2,3-dihydro-imidazo[1,2-a]pyridine-3-yl)-3-(4-nitro-phenyl)-imidazolidin-4-one (IMID4) and 2-[2-(4-Bromo-phenyl)-imidazo[1,2-a]pyridine-3-yl]-3-(4-methoxy-phenyl)-oxazolidin-5-one (OXAZ5) inhibitors

For each of (IMID4 and OXAZ5) three concentrations of (5, 10 and 20) ppm were prepared by dissolving (0.005, 0.01 and 0.02) gm, respectively in 6ml (DMSO), then transferred each one to (1L) volumetric flask containing 35gm (3.5%) of NaCl (dissolved in distilled water). The volume of each solution was completed to (1L) with the distilled water.

2.3. Electrochemical measurements

Potentiostatic polarization study

The potentiostat set up has included the following: a host computer with Mat lab software, magnetic stirrer, thermostat, potentiostat and galvanostat (Germany, 2000), The main part in apparatus is the corrosion cell; which was made out of Pyrex with (1L) capacity. This cell consisted of two bowls: external and internal. Three electrodes are mainly present in the electrochemical corrosion cell. Carbon steel specimen (with $1cm^2$) surface area which is represented the working electrode. This is used to determine the working electrode potential due to another electrode namely as reference electrode; located close to working electrode. A reference electrode was silver-silver chloride (Ag/AgCl, 3.0M KCl). The third electrode is a platinum auxiliary electrode with (10cm) length. The starting step was represented in immersing the working electrode in the test solution for fifteen minutes (15 min), to establish a steady state open circuit potential (E_{ocp}). This potential was noted for starting the electrochemical measurements in the range of (±200) mV. All tests solution were done at temperatures of (293, 303, 313 and 323) K.

2.4. Results and discussion

Quantum chemical calculations

The quantum electronic parameters are used to investigate the efficiency of corrosion inhibition such as: the highest occupied molecular orbital (E_{HOMO}), the energy of the lowest unoccupied molecular orbital (E_{LUMO}), the energy gap ($\Delta E_{HOMO-LUMO}$), electro-negativity (χ), dipole moment (μ), electron affinity (EA), ionization energy (IP), softness (S), global hardness (η), global electro-philicity (ω), the fraction of transferred electrons (ΔN) and the total energy (E_{tot}) [10].

Molecular structures calculations

The organic inhibitors compounds were built using Chem. Draw of Mopac program, see Figure-1. Gaussian 09 packages were used for calculating the fully optimize structure [8], see Figure-2, using quantum mechanical method of DFT of Becke's three-parameter of Lee, Yang and Parr (B3LYP) with 6-311++G (2d, 2p) level of the theory [11]. In addition to vacuum, the equilibrium geometry was calculated in two solvents of DMSO and H_2O.

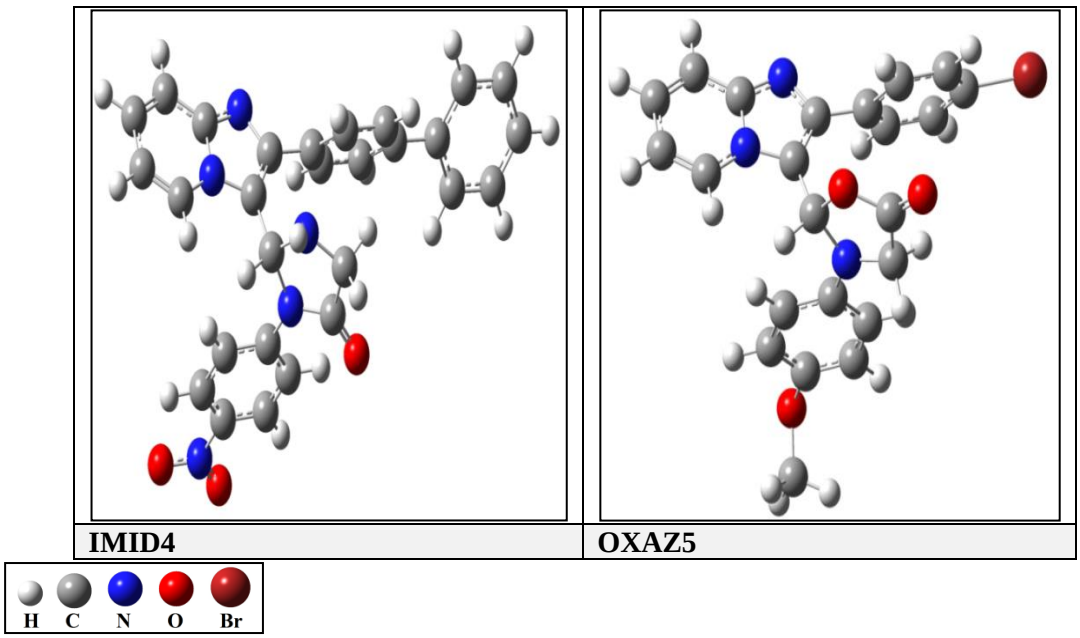

Figure 2-The three dimensions optimize structure of the two inhibition compound for the corrosion of carbon steel in sea waters;

Tables-(1, 2) display the geometrical structure (such as bond lengths, bond angles and dihedral angles) of the two inhibitors in vacuum and two solvents of (DMSO and H_2O). Figure-3 shows the numbering of atoms for the calculated inhibitors which calculated using DFT method. **C19-C20** (1.5129 Å) was the longest bond length and **N21-H** (1.00983 Å) was the shortest bond length found in IMID4 inhibitor. The bond angles were calculated between (103.1937 degree) for **N18C17N21** and (133.256 degree) for **C8C7C17**. For OXAZ5 inhibitor, **C13-Br** (1.916 Å) was the longest bond length and **C22-H** (1.0800 Å) was the shortest bond length. The bond angles were calculated between (104.845 degree) for **N17C18C19** and (132.563 degree) for **C3N4C7**. The values of the dihedral angles (trans & cis) for the two inhibitors showed that they are not planar (within C_1 point group) and the cis dihedral angles are not zero degree. All trans dihedral angles are more or less than 180.0 degree.

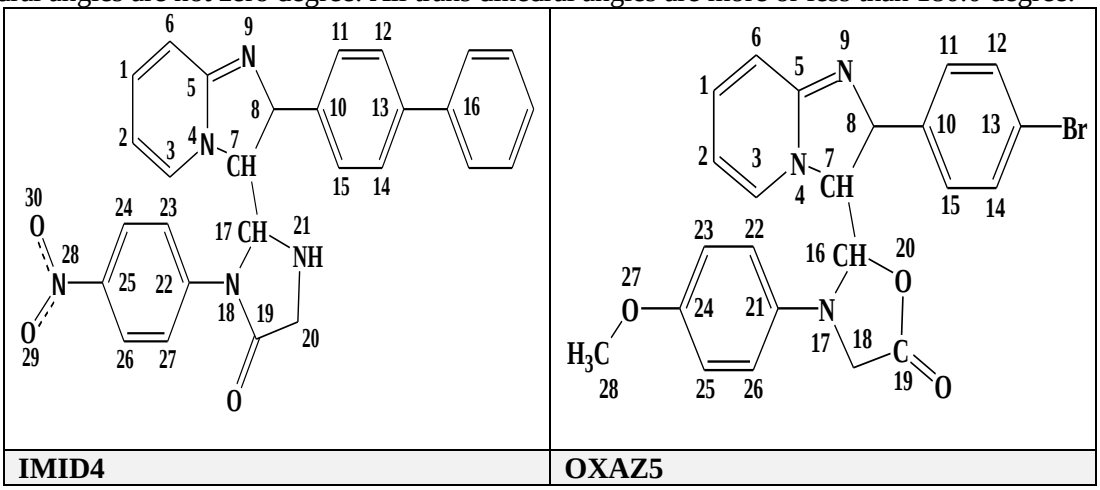

Figure 3-The numbering of atoms for two calculated inhibitors using for the corrosion of carbon steel in sea waters.

Table 1- The geometrical structure of compound IMID4 in vacuum and two solvents (DMSO, and H_2O) calculated using DFT method.

Description bond length	Bond length (Å)	Description angle	Angle (deg.)	Description dihedral angle	Dihedral angle (deg.)
C1-C2	1.42591	**C2C1C6**	120.01087	**HC1C2H**	-0.18606
C1-C6	1.37443	**C2C1H**	119.57821	**C6C1C2H**	179.61098
C1-H	1.07936	**C1C2C3**	120.81295	**HC2C3H**	-0.56685
C2-C3	1.36698	**C2C3N4**	119.55463	**C1C2C3H**	179.26020
C3-N4	1.38381	**N4C3H**	117.56144	**HC3N4C7**	1.02179
N4-C5	1.42011	**C3N4C7**	132.40062	**HC3N4C5**	-179.00058
N4-C7	1.40274	**C3N4C5**	120.92210	**C3N4C5C6**	-0.38316
C5-C6	1.41023	**C4C5N9**	110.40884	**C3N4C5N9**	179.43873
C5-N9	1.33981	**N9C5C6**	130.66968	**N9C5C6H**	0.28877
C7-C8	1.39429	**N4C7C8**	105.31342	**N4C5C6H**	-179.93131
C7-C17	1.50276	**C8C7C17**	133.25616	**N4C7C8N9**	-1.61803
C8-N9	1.38225	**C7C8N9**	111.24687	**N4C7C8C10**	177.72437
C8-C10	1.47558	**C7C8C10**	128.76870	**C7C8N9C5**	1.27813
C13-C14	1.40663	**C11C12C13**	121.12433	**C10C11C12H**	-179.38007
C17-N18	1.49936	**C12C13C16**	121.02586	**HC12C13C14**	177.97197
C17-N21	1.48299	**C14C15C10**	120.73840	**C16C13C14H**	-0.40503
C17-H	1.09239	**N18C17N21**	103.1937	**C12C13C14H**	179.52400
N18-C19	1.39275	**N18C17H**	108.5931	**HC14C15H**	1.54751
N18-C22	1.41653	**C19N18C17**	112.2036	**HC14C15C10**	-178.69437
C19-C20	1.51293	**C17N18C22**	123.1324	**HC17N18C22**	59.31058
C19-O	1.24056	**N18C19C20**	108.0054	**HC17N18C19**	-121.00957
C20-N21	1.46899	**N18C19O**	126.4053	**N18C19C20H**	123.16112
N21-H	1.00983	**C17N21C20**	110.6890	**N18C19C20N21**	1.97576
C22-C23	1.40967	**N18C22C23**	120.4717	**OC19C20N21**	-177.76416
C22-C27	1.41056	**N18C22C27**	120.5335	**N18C22C23H**	-0.53982
C23-C24	1.39013	**C22C23H**	120.8150	**N18C22C23C24**	-179.74419
C25-N28	1.45783	**C24C25C26**	121.2903	**HC24C25N28**	0.27818
C26-C27	1.38943	**C24C25N28**	119.2680	**HC24C25C26**	-179.61271
C26-H	1.07737	**C26C27C22**	120.8150	**N28C25C26H**	0.46300
N28-O29	1.27035	**O29N28O30**	120.2861	**N28C25C26C27**	179.93660
N28-O30	1.27148	**C25N28O29**	123.3757	**HC26C27H**	-0.38806

Table 2- The geometrical structure of compound OXAZ5 in vacuum and two solvents (DMSO and H_2O) calculated using DFT method.

Description bond length	Bond length (Å)	Description angle	Angle (deg)	Description dihedral angle	Dihedral angle (deg)
C1-C2	1.41816	**C2C1C6**	120.03044	**HC1C2H**	-0.47138
C1-C6	1.36800	**C2C1H**	119.57741	**HC1C2C3**	179.97916
C1-H	1.08001	**C1C2C3**	120.60608	**C1C2C3N4**	-0.41795
C2-C3	1.36129	**C2C3N4**	119.64724	**C1C2C3H**	178.68756
C3-N4	1.37303	**C3N4C7**	132.56396	**C2C3N4C5**	1.20483
N4-C5	1.40355	**C3N4C5**	121.19118	**C2C3N4C7**	-179.46964
N4-C7	1.39023	**N4C5C6**	118.90285	**C3N4C5C6**	-1.21204
C5-C6	1.40806	**N4C5N9**	111.04959	**C3N4C5N9**	178.73395
C5-N9	1.32776	**C5C6C1**	119.61042	**N4C5C6C1**	0.42816
C7-C8	1.38647	**N4C7C8**	105.21598	**N4C5C6H**	-179.63751
C7-C16	1.49349	**N4C7C16**	122.58440	**N4C7C8N9**	-1.34894
C8-N9	1.36108	**C7C8N9**	111.51652	**N4C7C8C10**	179.46063
C8-C10	1.48001	**C7C8C10**	128.29863	**C7C8N9C5**	0.89893
C10-C11	1.39615	**C8N9C5**	105.95809	**C10C8N9C5**	-179.83603
C13-Br	1.91765	**C12C13Br**	119.36469	**HC12C13Br**	-0.07526
C14-C15	1.39037	**C13C14C15**	119.02998	**BrC13C14C15**	-179.89669
C15-C10	1.39642	**C14C15C10**	120.89213	**BrC13C14H**	0.48437
C16-N17	1.47883	**C7C16O**	112.93854	**HC14C15H**	0.00083
C16-H	1.09070	**C7C16N17**	114.29324	**HC14C15C10**	179.50180
C16-O	1.45104	**C16N17C18**	111.90003	**C7C16N17C21**	-58.85837
N17-C18	1.41947	**C16N17C21**	123.64384	**C7C16N17C18**	120.93857
N17-C21	1.39858	**N17C18C19**	104.84507	**C16N17C18C19**	-0.47304
C18-C19	1.49948	**C18C19O20**	108.28759	**N17C18C19O**	-175.98134
C19-O	1.20899	**C19OC16**	110.73852	**N17C18C19O20**	3.53708
C19-O20	1.41277	**N17C21C22**	121.07857	**N17C21C22H**	-0.71947
C21-C22	1.40315	**N17C21C26**	120.33652	**N17C21C22C23**	179.61463
C22-H	1.07794	**C22C23C24**	119.68371	**HC23C24O**	0.72303
C24-C25	1.38744	**C23C24O**	119.53028	**OC24C25H**	-0.26828
C24-O	1.40948	**C24C25C26**	119.98347	**OC24C25C26**	179.07628
O27-C28	1.43360	**C24OC28**	111.86216	**HC25C26C21**	179.55982
C28-H	1.08469	**OC28H**	110.59542	**C24OC28H**	55.28257

Figure-4 shows the geometrical optimization of the studied inhibitors in vacuum including HOMO and LUMO density distributions. For (IMID4) inhibitor the HOMO is mainly located on (2-(2-Biphenyl-4-yl-imidazo [1,2-a] pyridine-3-yl)) moiety. This indicates that the preferred actives sites for an electrophilic attack are located within the region around the nitrogen atoms. Moreover, the electronic density of LUMO was distributed at the aromatic ring and around the ring of (4-nitro-phenyl) moiety (which is the most planar moiety in the molecule). For (OXAZ5) inhibitor, the HOMO

is mainly located on the imidazo[1,2-a] pyridine-3-yl]-3-(4-methoxy-phenyl)-oxazolidin-5-one moiety, and LUMO is located on the imidazo[1,2-a] pyridine-3-yl] moiety only.

LUMO	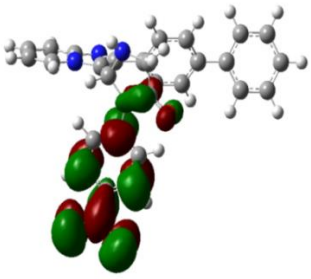	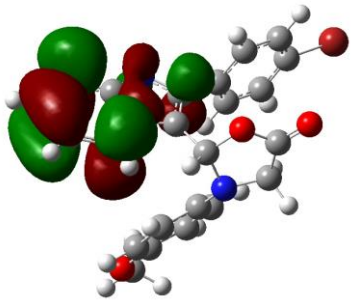
HOMO	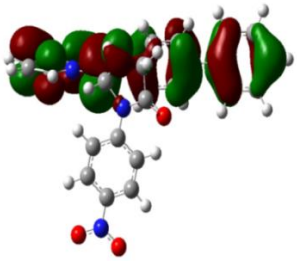 -	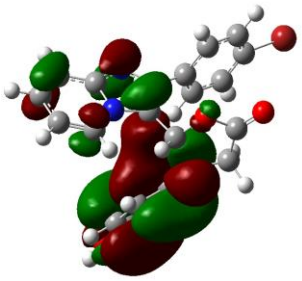
	IMID4	**OXAZ5**

Figure 4-Frontier Molecular Orbital density distributions for the calculated inhibitors using DFT method.

Global molecular reactivity

To study the influence of molecular geometry on the mechanism and efficiency of inhibition, the chemical quantum calculations for inhibition efficiency were performed. The quantum chemical parameters, such as: the energy of the highest occupied molecular orbital (E_{HOMO}), the energy of the lowest unoccupied molecular orbital (E_{LUMO}), energy gap ($\Delta E_{HOMO-LUMO}$), the dipole moment (μ), hardness (η), electro-negativity (χ), global softness (S), global electro-philicity index (**ω**) and electron transferred (ΔN), are all shown in Tables- (3a, 3b), (4a, 4b) for (IMID4) inhibitor and (OXAZ5) inhibitor, respectively.

Frontier orbital theory was used in predicting the adsorption centers of the inhibitor responsible of the reaction metal surface/molecule [12]. According to this theory, the formation of a transition state is due to an interaction between the Frontier orbital's (HOMO and LUMO) of the reactants. Parr et al. has introduced the index of global electro-philicity (ω) which is also related to the electron affinity (EA) and ionization potential (I.P) [4]. When interaction occurs between the inhibitor and the metal surface, flow of electrons takes place from the lower electronegativity molecule to the higher electronegativity metal, this transfer of electrons continues until the chemical potential becomes equal [4]. The electron transferred (ΔN) was calculated using theoretical (χ_{Fe}) and (η_{Fe}) values for mild steel of (7.0eV mol^{-1}) and (0.0eV mol^{-1}). The following Equations (1-8) are used for calculating the chemical parameters [13]:

$$IP \text{ (Ionization potential)} = -E_{HOMO} \quad (1)$$

$$EA \text{ (Electron-affinity)} = -E_{LUMO} \quad (2)$$

$$\Delta E = E_{LUMO} - E_{HOMO} \quad (3)$$

$$H \text{ (Hardness)} = (IE - EA)/ 2 \quad (4)$$

$$\chi \text{ (Electro-negativity)} = (IE + EA)/ 2 \quad (5)$$

$$S \text{ (Global softness)} = 1/ \eta \quad (6)$$

$$\text{Global electro-philicity index } (\boldsymbol{\omega}) = (-\chi)\, 2 \diagup 2\eta = \mu 2/ 2\eta \quad (7)$$

$$\text{Electron-transferred } (\Delta N) = (\chi_{Fe} - \chi_{inhib})/ [2 (\eta_{Fe} + \eta_{inhib.})] \quad (8)$$

Table 3a- DFT calculations for some physical properties of Imidazolidin-4-one derivative (IMID4**)** calculated at the equilibrium geometry.

Inhib. medium	P. G.	M. formula	E_{HOMO} (eV)	E_{LUMO} (eV)	$\Delta E_{HOMO-LUMO}$ (eV)	μ (Debye)	E_{total} (eV)
Vacuum	C_1	$C_{28}H_{23}N_5O_3$	**-6.299**	**-3.079**	**3.220**	**8.191**	**-42979.234**
DMSO	C_1		**-6.160**	**-3.364**	**2.796**	**11.363**	**-42979.979**
Water	C_1		**-6.159**	**-3.368**	**2.791**	**11.423**	**-42979.990**

Table 3b- DFT quantum chemical parameters for Imidazolidin-4-one derivative (IMID4**)** calculated at the equilibrium geometry.

Inhib. medium	IP (eV)	EA (eV)	η (eV)	χ (eV)	S (eV)	ω (eV)	ΔN
Vacuum	**6.299**	**3.079**	**1.61**	**4.689**	**0.621**	**6.829**	**0.717**
DMSO	**6.160**	**3.364**	**1.398**	**4.762**	**0.715**	**8.110**	**0.800**
Water	**6.159**	**3.368**	**1.395**	**4.763**	**0.716**	**8.131**	**0.801**

Table 4a- DFT calculations for some physical properties of Oxazolidin-5-one derivative (OXAZ5**)** calculated at the equilibrium geometry.

Inhib. medium	P. G.	M. formula	E_{HOMO} (eV)	E_{LUMO} (eV)	$\Delta E_{HOMO-LUMO}$ (eV)	μ (Debye)	E_{total} (eV)
Vacuum	C_1	$C_{23}H_{20}N_3O_3Br$	**-5.908**	**-1.708**	**4.200**	**6.224**	**-104812.558**
DMSO	C_1		**-5.797**	**-1.515**	**4.282**	**8.469**	**-104813.086**
Water	C_1		**-5.796**	**-1.514**	**4.282**	**8.509**	**-104813.094**

Table 4b- DFT quantum chemical parameters for Oxazolidin-5-one derivative (OXAZ5**)** calculated at the equilibrium geometry.

Inhib. medium	IP (eV)	EA (eV)	η (eV)	χ (eV)	S (eV)	ω (eV)	ΔN
Vacuum	**5.908**	**1.708**	**2.1**	**3.808**	**0.476**	**3.452**	**0.76**
DMSO	**5.797**	**1.515**	**2.141**	**3.656**	**0.467**	**3.121**	**0.780**
Water	**5.796**	**1.514**	**2.141**	**3.655**	**0.467**	**3.119**	**0.781**

The active sites of the two inhibitors:

The inhibition of the studied inhibitors was determined via DFT Mulliken charges population analysis; which gave an indication of the reactive centers of the molecules (electrophilic and nucleophilic centers). For that, region that have a large electronic charge are chemically softer than the region that have a small electronic charge. Thus, the density of electron may play an important role in the chemical reactivity calculating. The chemical adsorption interactions are either by orbital interactions or by electrostatic. The nucleophilic attack sites will be the place where the positive charge value is a maximum, and hence, only the charges on the oxygen (O), nitrogen (N) and some carbon atoms would be present. The electrophilic attack site was controlled by the negative charge value.

The nucleophilic and electrophilic electronic charge values of the two inhibitors are found to be greater in the solutions of DMSO and H_2O than in vacuum, this is shown in Tables- (5, and 6) for IMID4 and OXAZ5, respectively.

The orders of the nucleophihic reactive sites of IMID4 inhibitor were found to be as: C14> C12> C15> C1> C2> N9> N20> C8> C7 and the electrophihic reactive sites order were found to be as: C5> C13> C16> C10> C22> C19

For OXAZ5 inhibitor, the orders of the nucleophihic reactive sites of OXAZ5 inhibitor were found to be as: C24> O27> O20> C14> C1> N9> C12> C7> C2 and the electrophihic reactive sites order are: C5> C19> C16.

Table 5- DFT Mulliken charges population analysis for IMID4 molecule in three media of (vacuum, DMSO, and H_2O).

Atom no.	Electronic charge/ ecu	Atom no.	Electronic charge/ ecu	Atom no.	Electronic charge/ ecu	Atom no.	Electronic charge/ ecu
C_1	-0.310V -0.333D -0.334H	N_9	-0.228V -0.358D -0.350H	C_{16}	0.744V 0.679D 0.678H	C_{23}	-0.137V -0.112D -0.112H
C_2	-0.288V -0.350D -0.351H	C_{10}	0.499V 0.486D 0.485H	C_{17}	-0.094V -0.103D -0.103H	C_{24}	-0.294V -0.290D -0.290H
C_3	-0.074V -0.034D -0.033H	C_{11}	-0.191V -0.212D -0.213H	N_{18}	-0.075V -0.044D -0.044H	C_{26}	-0.158V -0.196D -0.198H
N_4	0.135V 0.131D 0.131H	C_{12}	-0.484V -0.491D -0.491H	C_{19}	0.225V 0.262D 0.263H	C_{27}	-0.167V -0.174D -0.174H
C_5	0.692V 0.694D 0.694H	C_{13}	0.696V 0.603D 0.601H	C_{20}	-0.075V -0.071D -0.070H	N_{28}	-0.054V -0.004D -0.003H
C_7	-0.205V -0.199D -0.199H	C_{14}	-0.528V -0.521D -0.521H	N_{21}	-0.261V -0.302D -0.303H	O_{29}	-0.129V -0.189D -0.190H
C_8	-0.380V -0.273D -0.271H	C_{15}	-0.491V -0.485D -0.484H	C_{22}	0.472V 0.459D 0.459H	O_{30}	-0.131V -0.188D -0.188H

V: Vacuum, D: Dimethyl sulfoxide (DMSO), H: Water, ecu: electron control unit.

Table 6- DFT Mulliken charges population analysis for OXAZ5 molecule in three media of (vacuum, DMSO, and H_2O).

Atom no.	Electronic charge/ ecu	Atom no.	Electronic charge/ ecu	Atom no.	Electronic charge/ ecu	Atom no.	Electronic charge/ ecu
C_1	-0.324V -0.343D -0.343H	N_9	-0.253V -0.373D -0.375H	C_{15}	-0.260V -0.284D -0.285H	C_{23}	0.043V 0.044D 0.044H
C_2	-0.202V -0.267D -0.268H	C_{10}	0.279V 0.302D 0.302H	C_{16}	0.206V 0.194D 0.193H	C_{24}	-0.712V -0.656D -0.655H
C_3	-0.108V -0.056D -0.055H	C_{11}	-0.012V -0.047D -0.047H	N_{17}	-0.041V -0.028D -0.027H	C_{25}	-0.057V -0.000D -0.001H
N_4	0.170V 0.168D 0.168H	C_{12}	-0.273V -0.311D -0.312H	C_{18}	0.154 V 0.119D 0.118H	C_{26}	-0.056V -0.064D -0.064H
C_5	0.529V 0.539D 0.539H	C_{13}	0.075V 0.071D 0.071H	C_{19}	0.213V 0.292D 0.293H	O_{27}	-0.369V -0.418D -0.419H
C_7	-0.306V -0.287D -0.286H	C_{14}	-0.334V -0.361D -0.361H	O_{20}	-0.333V -0.366D -0.367H	C_{28}	-0.087 V -0.081D -0.081H

V: Vacuum, D: Dimethyl sulfoxide (DMSO), H: Water, ecu: electron control unit.

Corrosion inhibition measurement

Potentiodynamic Polarization Measurements.

Tables-(7, and 8) show the electrochemical corrosion parameters, such as: corrosion current density ($I_{corr.}$), corrosion potential ($E_{corr.}$) and Tafel slopes (ba and/or bc) for the two inhibitors [14]. Figure-3 presents potentiodynamic polarization curves for carbon steel in salt media containing different conditions of the two inhibitors. Corrosion efficiency (IE%) and the surface coverge (**Θ)** were measured using Equations (9, 10):

$$\%\mathbf{IE} = \frac{I_{corr(un)} - I_{corr(in)}}{I_{corr(un)}} \times 100 \quad \ldots . (\mathbf{9})$$

Where $I_{corr\ (in)}$ is the inhibited corrosion current densities, $I_{corr\ (un)}$ is the uninhibited current densities.

$$\mathbf{\Theta} = \frac{\%\mathbf{IE}}{100} \quad (\mathbf{10})$$

The addition of the two derivatives cause a reduce in the corrosion rate (CR), i.e. shifts the cathodic and anodic curves to lower values of ($I_{corr.}$), and both cathodic and anodic reactions of carbon steel electrode corrosion inhibited by the two organic compounds in saline media. Figure-5 shows the polarisation curve for the corrosion of carbon steel in the salt solution, with and without the addition of IMID4 inhibitor at various concentrations, and at the optimum conditions of (20ppm) with temperature of (293K). Figure-6 shows the polarisation curve for the corrosion of carbon steel in the salt solution with and without the addition of OXAZ5 inhibitor at various concentrations, and with the optimum conditions of (20ppm) and at temperature of (293K).

Tables- (7, and 8) show that the increase in temperature led to increase ($I_{corr.}$), while the efficiencies IE% enhance with the increase the inhibitor concentration. The optimum conditions for IMID4 in the salt solution were observed at (293K and 20ppm); which corresponded to the lowest $I_{corr.}$(14.52 $\mu A.cm^{-2}$) and maximum IE% (89.093%, while OXAZ5 inhibitor have the optimum conditions at 293K and 20ppm too, this corresponded to lowest $I_{corr.}$(25.33 $\mu A.cm^{-2}$) and maximum IE% (80.973 %). The values of iron CR have decreased with increasing the concentration of the inhibitors and the addition of inhibitor to the blank solutions have led to increase the cathodic and anodic I_{corr} without shifting the E_{corr}. So, the two inhibitors can be described as mixed-type inhibitors. Inhibition occurred by adsorption and the inhibition effect results from the reduction corrosion reaction on the carbon steel surface area [15].

Table 7- Electrochemical data of C.S corrosion in sea water at different concentrations for IMID4 compound.

Soln.	T (K)	E_{corr} (mV)	I_{corr} ($\mu A.cm^{-2}$)	Bc ($mV.dec^{-1}$)	ba ($mV.dec^{-1}$)	IE%	Θ	CR $mm.y^{-1}$
Blank 3.5% NaCl	293	-408.0	133.13	-230.4	138.5	------	------	33.15
	303	-446.7	172.04	-279.6	110.2	------	------	42.84
	313	-491.2	189.34	-269.0	96.5	------	------	47.15
	323	-547.7	192.99	-252.9	84.4	------	------	48.05
5ppm	293	-358.8	18.07	-47.7	43.7	86.426	0.864	4.50
	303	-421.2	37.49	-97.9	55.5	78.208	0.782	9.34
	313	-439.2	49.76	-93.0	58.0	73.719	0.737	12.39
	323	-518.0	52.95	-93.2	52.6	72.563	0.726	13.18
10ppm	293	-388.7	15.51	-97.6	58.7	88.349	0.883	3.86
	303	-426.3	22.92	-63.8	38.8	86.677	0.867	5.71
	313	-453.6	47.75	-99.4	56.0	74.780	0.748	11.89
	323	-489.1	66.25	-115.6	64.4	65.671	0.657	16.50
20ppm	293	-356.1	14.52	-62.8	43.9	89.093	0.891	3.62
	303	-439.9	31.99	-119.6	45.7	81.405	0.814	7.97
	313	-527.4	35.81	-160.4	64.4	81.086	0.811	8.92
	323	-548.9	38.40	-147.5	65.7	80.102	0.801	9.56

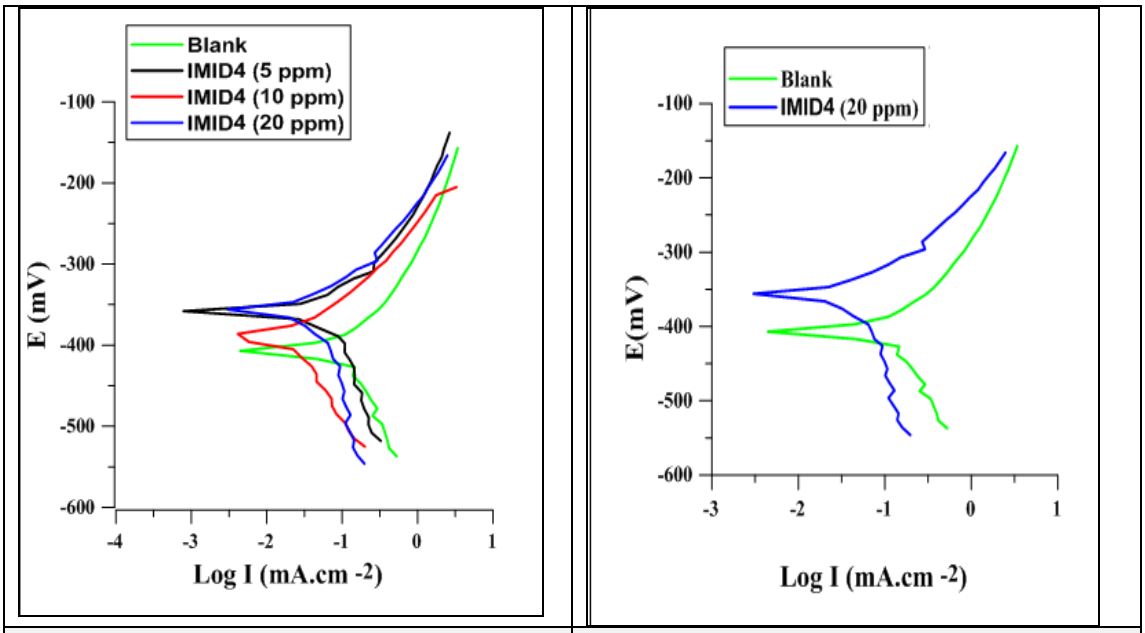

Figure 5- Polarisation curve of C.S in sea water for (IMID4) compound (a) at different concentrations and T (of 293K), and (b) at the optimum concentration and T (of 293K).

Table 8- Electrochemical data of the C.S corrosion in sea water at different concentrations for OXAZ5 compound.

Solun.	T (K)	E_{corr} (mV)	I_{corr} ($\mu A.cm^{-2}$)	bc ($mV.dec^{-1}$)	ba ($mV.dec^{-1}$)	IE%	Θ	CR $mm.y^{-1}$
Blank 3.5% NaCl	293	-408.0	133.13	-230.4	138.5	------	------	33.15
	303	-446.7	172.04	-279.6	110.2	------	------	42.84
	313	-491.2	189.34	-269.0	96.5	------	------	47.15
	323	-547.7	192.99	-252.9	84.4	------	------	48.05
5ppm	293	-504.2	31.53	-182.6	71.5	76.316	0.763	7.85
	303	-630.7	41.68	-175.6	68.8	75.773	0.758	10.38
	313	-662.8	50.77	-257.3	71.6	73.185	0.732	12.64
	323	-712.4	55.77	-365.4	72.2	71.102	0.711	13.89
10ppm	293	-533.1	27.72	-171.2	77.8	79.178	0.792	6.90
	303	-651.6	36.45	-300.1	74.0	78.813	0.788	9.08
	313	-670.5	42.18	-245.9	72.3	77.722	0.777	10.50
	323	-744.4	46.86	-343.0	88.7	75.718	0.757	11.67
20ppm	293	-491.4	25.33	-90.0	48.2	80.973	0.810	6.31
	303	-524.1	34.10	-70.3	49.1	80.179	0.802	8.49
	313	-582.2	40.01	-93.9	57.4	78.868	0.789	9.96
	323	-612.6	44.68	-95.8	53.6	76.848	0.768	11.13

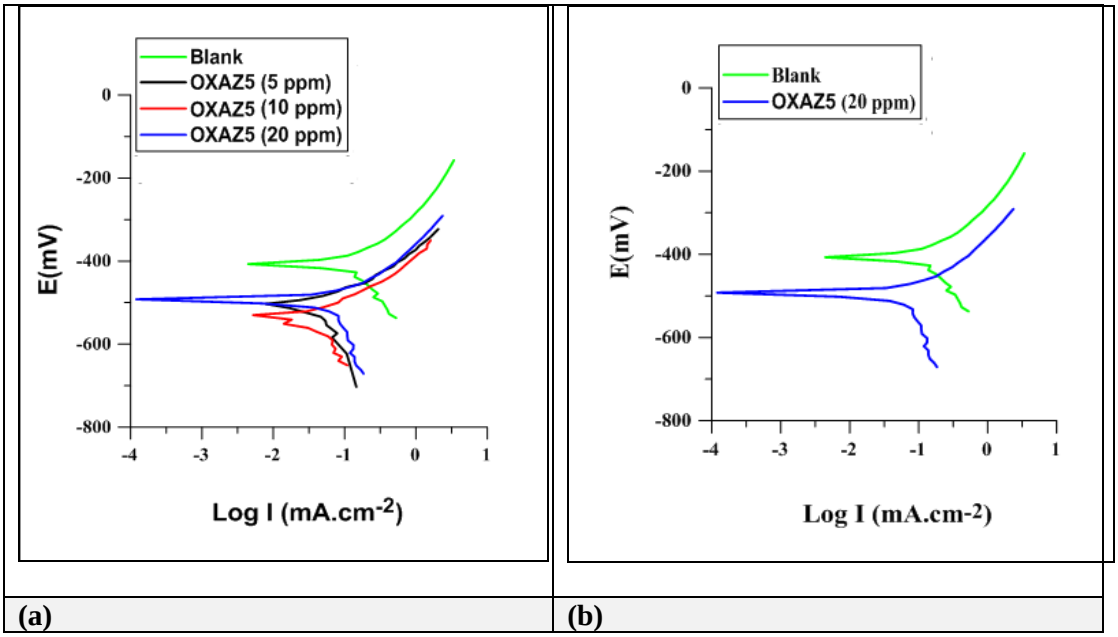

Figure 6- Polarisation curve of C.S in sea water for (OXAZ5) compound (a); at different concentrations and T (of 293K) and (b); at the optimum concentration and T (of 293K).

Kinetic and thermodynamic activation parameters for corrosion processes

Figures-(7, and 9) shown the straight line plots between log I_{corr} and 1/T for (IMID4) and (OXAZ5) inhibitors respectively. The Arrhenius law is presented as a straight line of the logarithm of the corrosion rate. The activation parameters were calculated with and without inhibitors at different concentrations. The activation energy of the corrosion process (E_a), and the pre-exponential factor (*A*), were calculating from Equations 11. A plot of log (CR/ T) against (1/T) or log (I_{corr}/T) against (1/T), Equation (12) gave a linear relationship with a slope of (−ΔH*/ 2.303R) and an intercept of [log(R/ Nh)+ (ΔS*/ 2.303R)]. This is shown in Figures- (8, and 10) for (IMID4) and (OXAZ5) inhibitors, respectively.

$$\text{Log (Icorr)} = \text{Log } A - \text{Ea}/\ 2.303RT \quad (11)$$

$$\text{Log (Icorr/ T)} = \log (\text{CR/ T}) = \text{Log (R/ N h)} + \Delta S^*/\ 2.303R - \Delta H^*/\ 2.303RT \quad (12)$$

Where (I_{corr}) is the corrosion current density which is equal to the corrosion rate (CR), (R) is the universal gas constant (8.314 J mol^{-1} K^{-1}), (T) is the absolute temperature in K, (h) is Planck's constant (6.626 x 10^{-34} J s), (N) is Avogadro's number (6.022 x 10^{23} mol^{-1}), ΔH* is the enthalpy of activation and ΔS*, is the entropy of activation. Accordingly, the activation thermodynamic parameters (ΔH* and ΔS*) were calculated for (IMID4) and (OXAZ5) inhibitors, respectively, as shown in Tables- (9, and 10). (ΔH*) values for the corrosion reaction in 3.5% NaCl at the temperature range of (293-323) K and different concentration were found to be positive values for both inhibitors; which may give an indication of an endothermic nature for this reaction [16]. Negative values of (ΔS*) for the corrosion reaction indicate a decrease in the degree of freedom and a consequent inhibition action [17]. The values of ΔG* for corrosion reaction were calculated from equation 13. The positive values of ΔG* indicating that the transition state of the adsorption process is not spontaneous, (see Tables- 9, 10).

$$\Delta G^* = \Delta H^* - T\ \Delta S^* \quad (13)$$

Table 9- Corrosion kinetic parameters for carbon steel in sea water (3.5% NaCl) for blank with various concentrations of (IMID4) inhibitor.

Conc. (ppm)	ΔG (kJ/ mol)				ΔH* kJ/ mol	ΔS* kJ/ mol K	Ea kJ/ mol	*A* Molecule/ cm^2 S
	293K	303K	313K	323K				
Blank	63.042	64.932	66.862	68.772	7.079	-0.191	9.636	1.10305E+27
5	67.372	69.012	70.452	71.892	25.380	-0.144	27.936	3.03417E+29
10	68.560	69.620	70.680	71.740	37.502	-0.106	40.060	3.09272E+31
20	68.235	69.825	71.415	72.005	21.648	-0.159	24.204	5.45683E+28

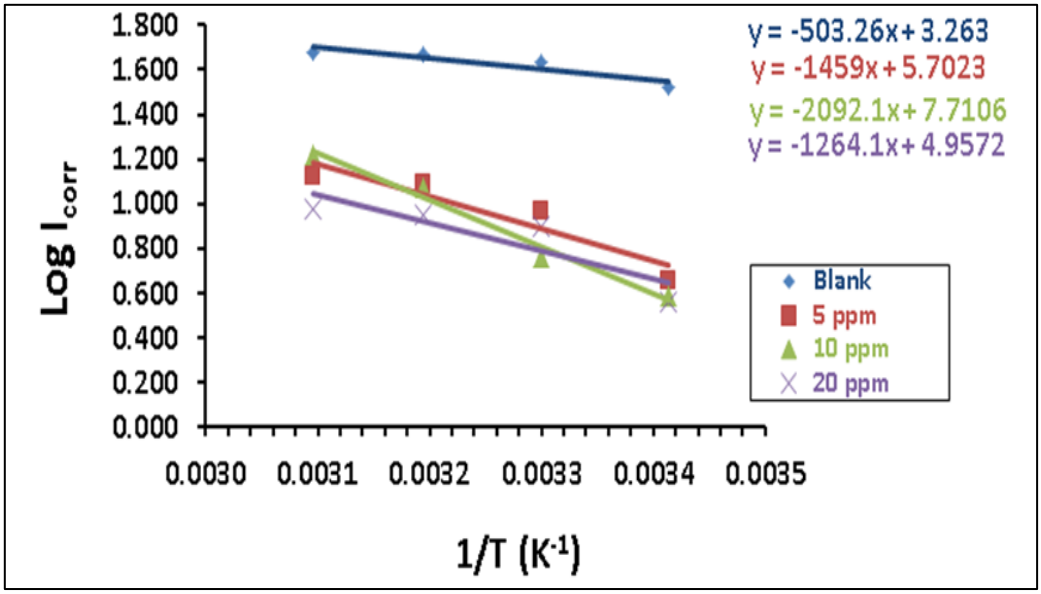

Figure 7- Plot of log (Icorr) vs. (1/ T) for carbon steel in sea water for blank and in presence of different concentrations of the **(**IMID4) compound.

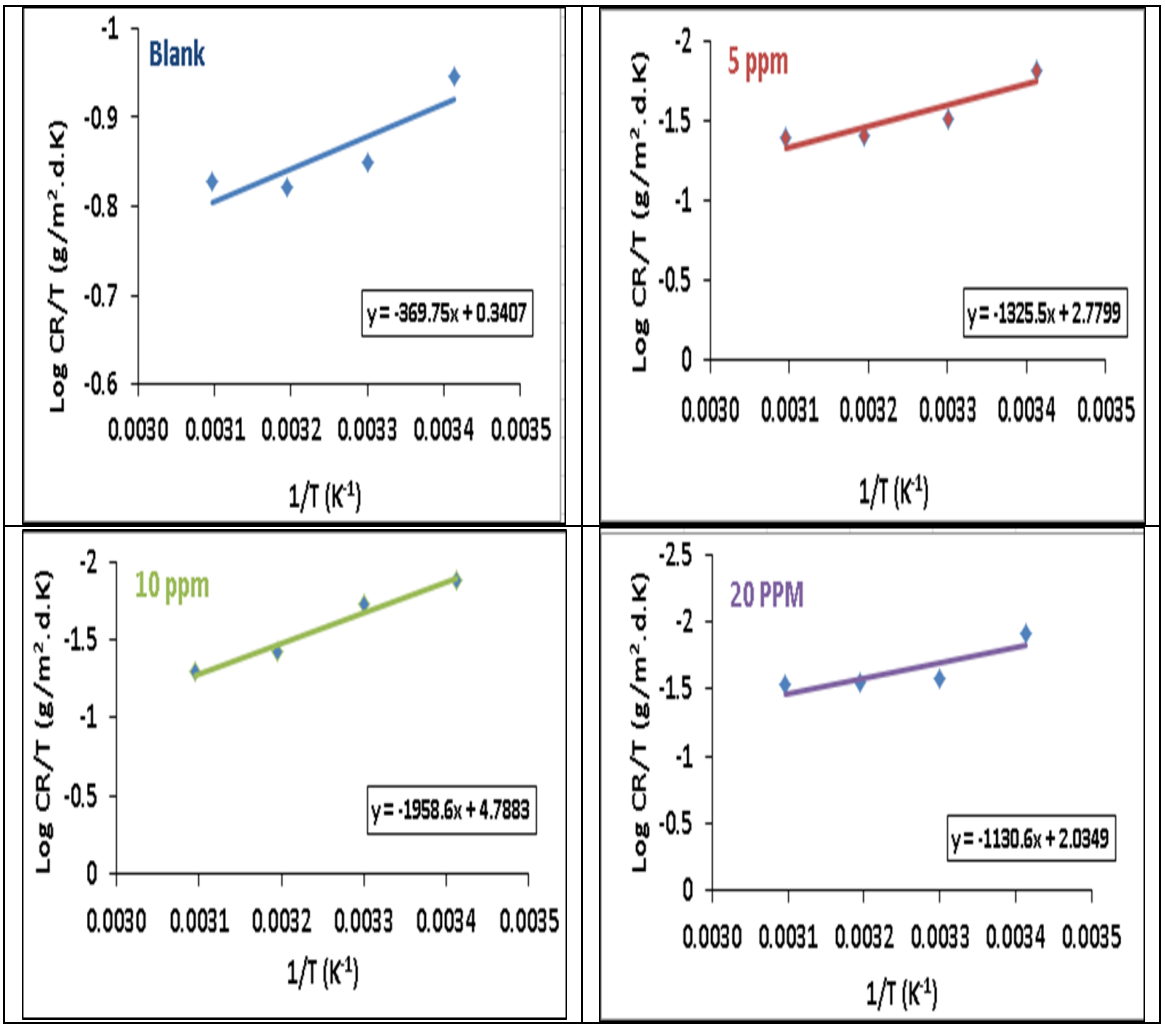

Figure 8- Plot for log (CR/ T) vs (1/T) for carbon steel in sea water for blank and in presence of different concentration of (IMID4) compound.

Table 10- Corrosion kinetic parameters for carbon steel in sea water for blank and with various concentrations of (OXAZ5) inhibitor.

Conc. (ppm)	ΔG* kJ/ mol				ΔH* kJ/ mol	ΔS* kJ/ mol K	Ea kJ/ mol	*A* Molecule/ cm^2 S
	293K	303K	313K	323K				
Blank	63.042	64.952	66.862	68.772	7.079	-0.191	9.635	1.10305E+27
5	66.750	68.600	70.450	72.300	12.545	-0.185	15.102	2.41402E+27
10	67.092	68.439	70.849	72.759	11.065	-0.191	13.622	1.1862E+27
20	67.901	69.151	71.031	72.911	12.187	-0.188	14.744	1.68438E+27

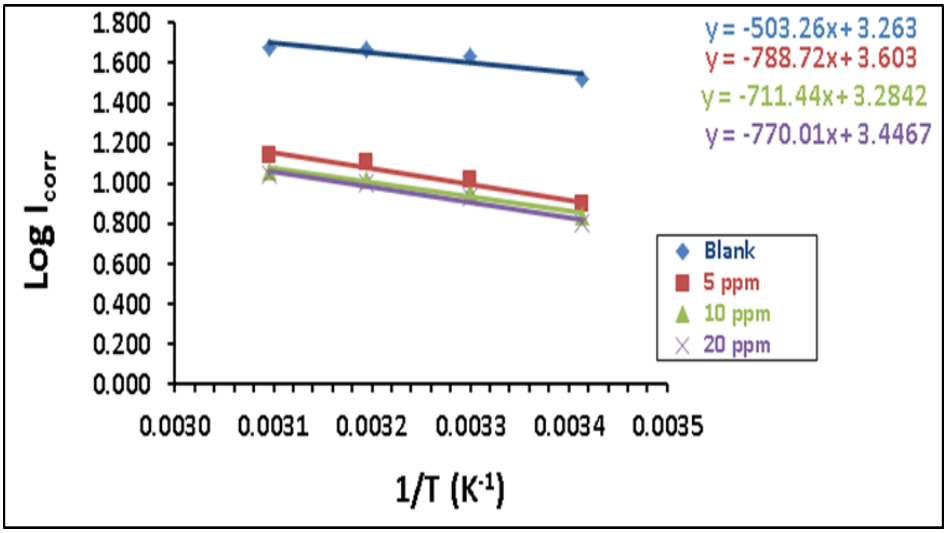

Figure 9- Plot for log (Icorr) vs. (1/ T) for carbon steel in sea water for blank and in presence of different concentrations of (OXAZ5) compound.

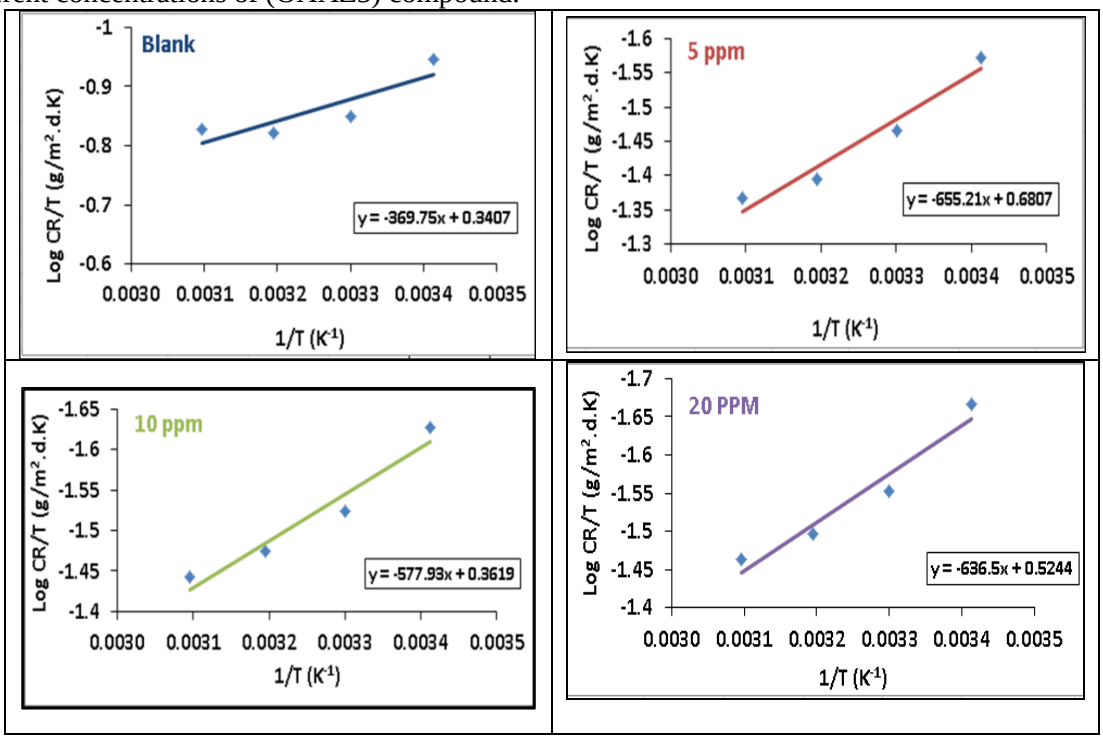

Figure 10-Plot of log (CR/ T) vs. (1/T) for carbon steel in saline water for blank and in presence of different concentrations of **(**OXAZ5) inhibitor compound.

Adsorption isotherm

Adsorption isotherms are necessary to elucidate the corrosion inhibition mechanism since they express the interaction between the inhibitor molecules and the active sites on the carbon steel surface. In this study, the results were based on the Langmuir isotherm; see Figures-(12, 14) for (IMID4) inhibitor and (OXAZ5) inhibitor, respectively. Langmuir adsorption isotherm can be expressed by Equation (14) as follows [18]:

$$C/\Theta = (1/K_{ads}) + C\ldots \quad (14)$$

Whereas C is the inhibitor concentration in 3.5% NaCl and K_{ads} is the adsorption/ desorption equilibrium constant. A plot of C/θ versus C in the salt media, could be used to determine the equilibrium adsorption constant K_{ads}. Further the standard free energy change $\Delta G°_{ads}$ values for the adsorption are calculated using Equation 15.

$$K_{ads} = (1/55.55) \exp(-\Delta G°_{ads}/RT) \quad (15)$$

Where K is the equilibrium constant, R is the universal gas constant and T is the absolute temperature and 55.5 is the concentration of water in solution in mol/dm^3. The negative values of $\Delta G°_{ads}$ ensured the spontaneity of the adsorption process and stability of the adsorbed layer on the carbon steel surface. The enthalpy and entropy for the adsorption of
(IMID4 and (OXAZ5) on mild steel are deduced by using the thermodynamic Equation of (16).

$$\Delta G°_{ads} = \Delta H°_{ads} - T\Delta S°_{ads} \quad (16)$$

$\Delta H°_{ads}$ can be also deduced from the integrated version of the Vant_Hoff equation expressed by:

$$\text{Ln } K = -\Delta H°_{ads}/RT + \text{constant} \quad (17)$$

Figures-(14, 16) and Tables- (11, 12) show the thermodynamic functions of the adsorption process for (IMID4 and (OXAZ5) inhibitors.

The negative values of $\Delta G°_{ads}$ reflect the spontaneous adsorption. Generally, the values of $\Delta G°_{ads}$ around -20 kJ mol^{-1} or more positive are consistent with physisorption, while those around -40 kJ mol^{-1} or more negative with chemisorptions [19]. The calculated values of $\Delta G°_{ads}$ were found to be in the range of (-13.640 to -8.221kJ mol^{-1}) and (-11.575 to -11.155kJ mol^{-1}) at temperatures of (293 to 323K) for (IMID4 and OXAZ5) inhibitors respectively. The entropy $\Delta S°_{ads}$ value was positive confirming that the increase in disordering takes place on going from the reactant to the adsorbed species [15]. The negative sign of $\Delta H°_{ads}$ in salt media indicated that the adsorption of inhibitor molecules is an exothermic and physisorption process. For IMID4 inhibitor, $\Delta H°_{ads}$ was found to be (-68.393kJ mol^{-1}), and it was found to be (-5.692kJ mol^{-1}) for (OXAZ5).

Table 11- Thermodynamic parameters for (IMID4) adsorption on carbon steel surface in 3.5% NaCl at different temperatures

T (K)	K_{ads} (L mol^{-1})	$\Delta G°_{ads}$ (kJ. mol^{-1})	$\Delta H°_{ads}$ (kJ.mol^{-1})	$\Delta S°_{ads}$(kJ.mol^{-1})	R^2
293	2.112 x 10^6	-13.640	-68.393	0.141	1.000
303	3.850 x 10^6	-15.127			0.996
313	4. 196 x 10^6	-9.634			0.998
323	4.972 x 10^6	-8.221			0.979

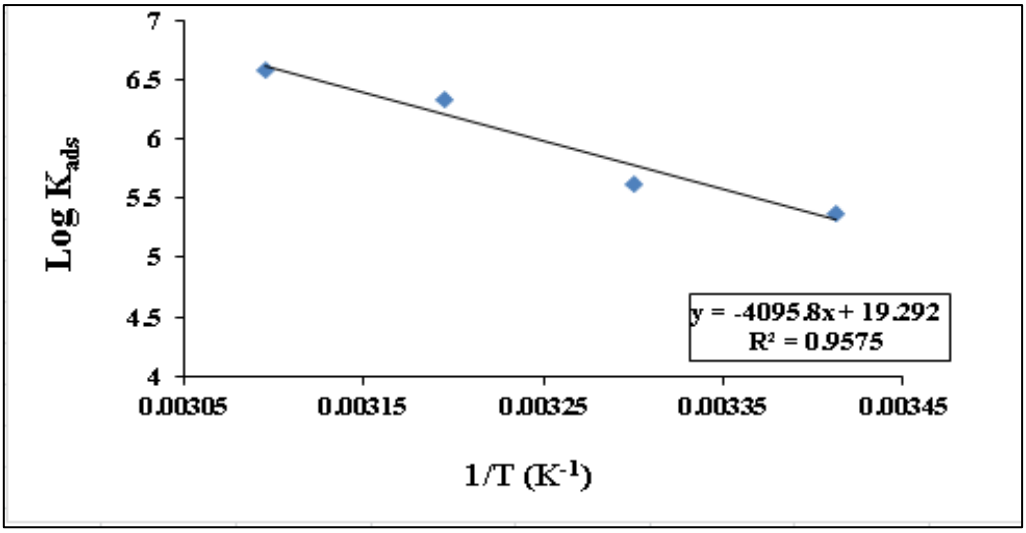

Figure 11- Plot of log Kadsvs (1/ T) for (IMID4) inhibitor.

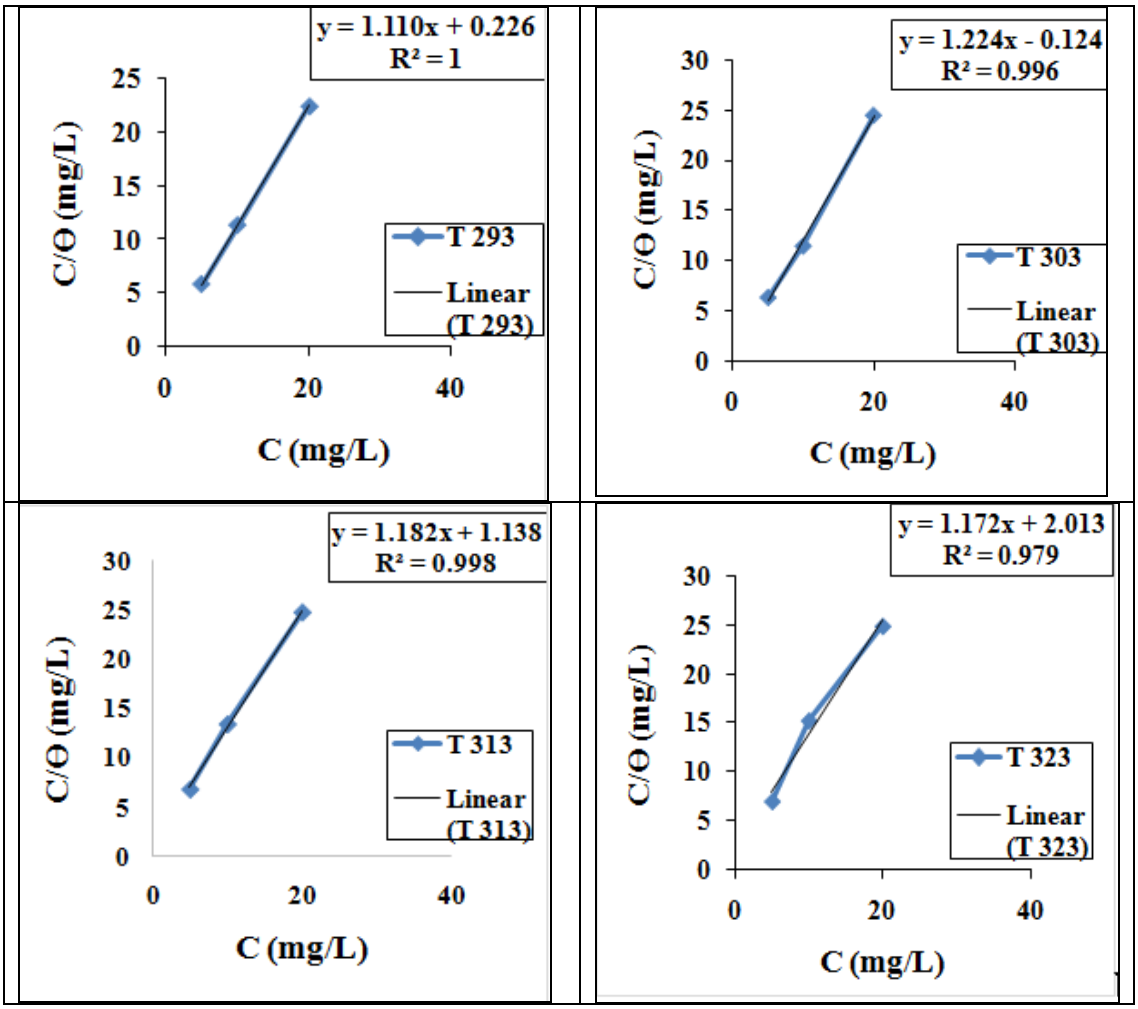

Figure 12- Langmuir isotherms plot for the (IMID4) adsorption on carbon steel surface in the saline media at the temperature range of (293, 303, 313 and 323) K

Table 12-Langmuir parameters for the adsorption of (OXAZ5) organic compound on carbon steel surface in sea water solutions at different temperatures.

T (K)	K_{ads} (L mol^{-1})	$\Delta G°_{ads}$ (kJ. mol^{-1})	$\Delta H°_{ads}$ (kJ.mol^{-1})	$\Delta S°_{ads}$(kJ.mol^{-1})	R^2
293	7.570 x 10^5	-11.975	-5.692	0.128	1.000
303	8.967 x 10^5	-11.815			1.000
313	9.879 x 10^5	-11.258			0.999
323	9.890 x 10^5	-11.155			0.999

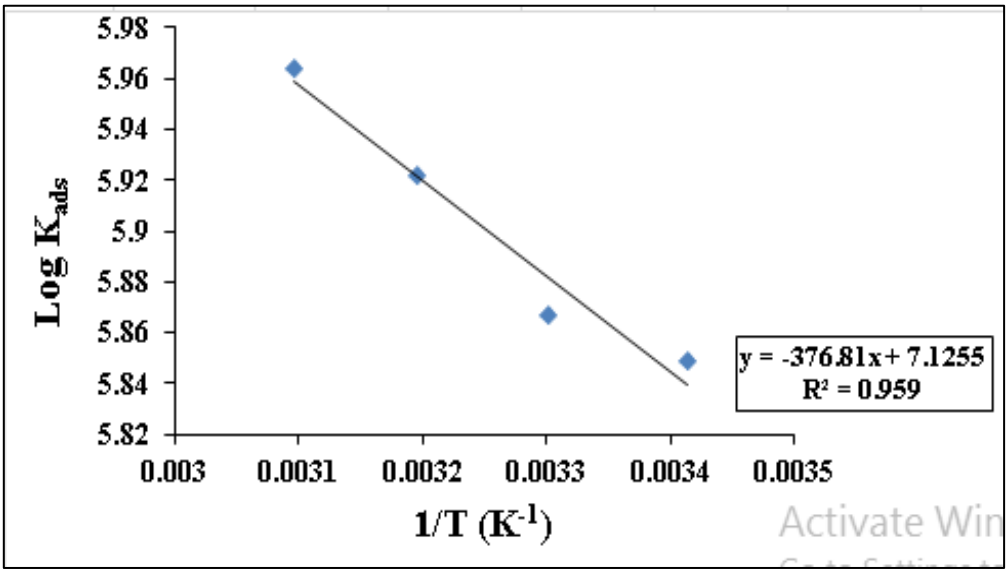

Figure 13- Plot of (log K_{ads}) vs (1/ T) for (OXAZ5) inhibitor.

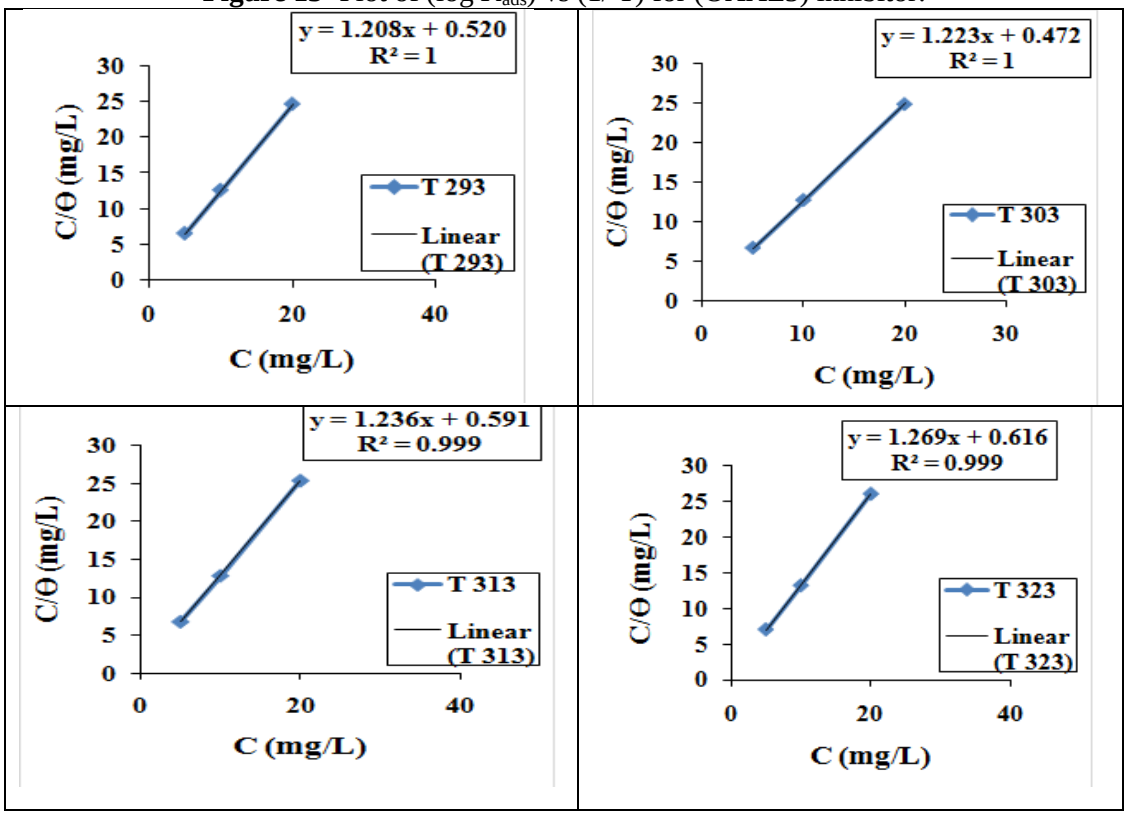

Figure 14- Langmuir isotherms plot for the adsorption compound **(**OXAZ5**)** on C.S in saline solution at the temperature range of (293, 303, 313 and 323)K.

Scanning Electron Microscopy (SEM)

Figures- (15a, 16a), show the damaged surface of carbon steel obtained when the metal was remained immersed in saline water without (IMID4) and (OXAZ5) inhibitors, respectively. However, Figures- (15b, 16b) show the smoothness and regularity on the surface of carbon steel in the presence of (IMID4) and (OXAZ5) inhibitors, respectively, in saline water when compared to Figures- (15a, 16a); which indicated the reduction of the surface corrosion. This improvement in the surface morphology is due to the formation of protective films of inhibitors (IMID4) and (OXAZ5) on the carbon steel surface, and hence, indicated the inhibition of the corrosion [20].

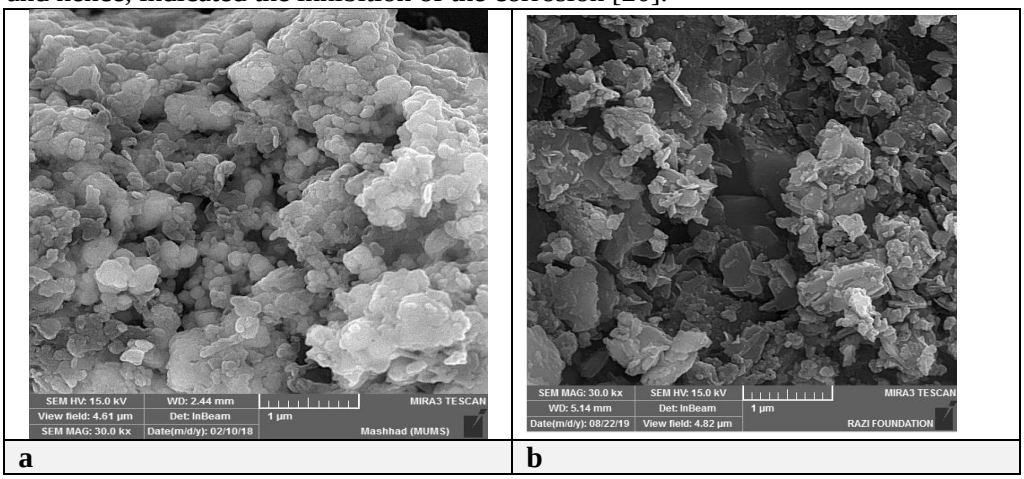

Figure 15- SEM images of C.S in a 3.5% NaCl saline solution at 293K (a) without (IMID4), (b) In the presence of 20 ppm of the organic compound (IMID4).

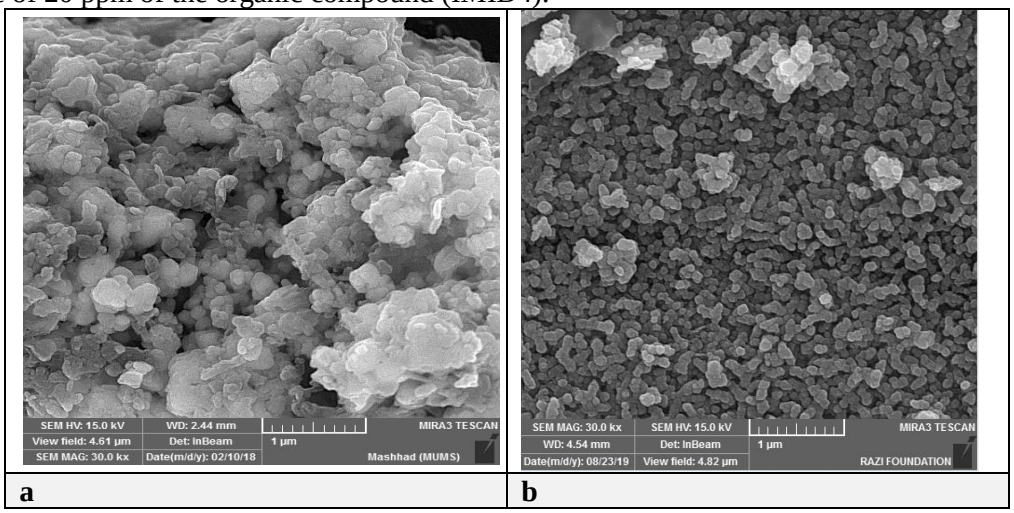

Figure 16- SEM images of carbon steel in a 3.5% NaCl saline solution at 293K (a); without (OXAZ5) and (b); In the presence of 20 ppm of the organic compound of (OXAZ5).

Atomic Force Microscopy (AFM)

The surface morphology of carbon steel samples in a saline solution of 3.5% NaCl in absence and presence of the optimum concentration (20 ppm) of the two inhibitors were investigated by AFM. The results are shown in Figures- (17(a-f)). The average roughness is shown in Figures- (17(a, b))), indicated that the C.S samples surface is badly damaged due to 3.5% NaCl salt attack. The average roughness (S_a) for the carbon steel surface is 3.97nm in salt solution without the presence of any inhibitor [21]. (S_a) was reduced to 2.53nm in the presence of the optimum concentration (20 ppm) of compound (IMID4) Figures- (17 (c,d)), and it was reduced to 2.26nm in the presence of the optimum concentration (20 ppm) of **(**OXAZ5) inhibitor Figures- (17 (e,f)).

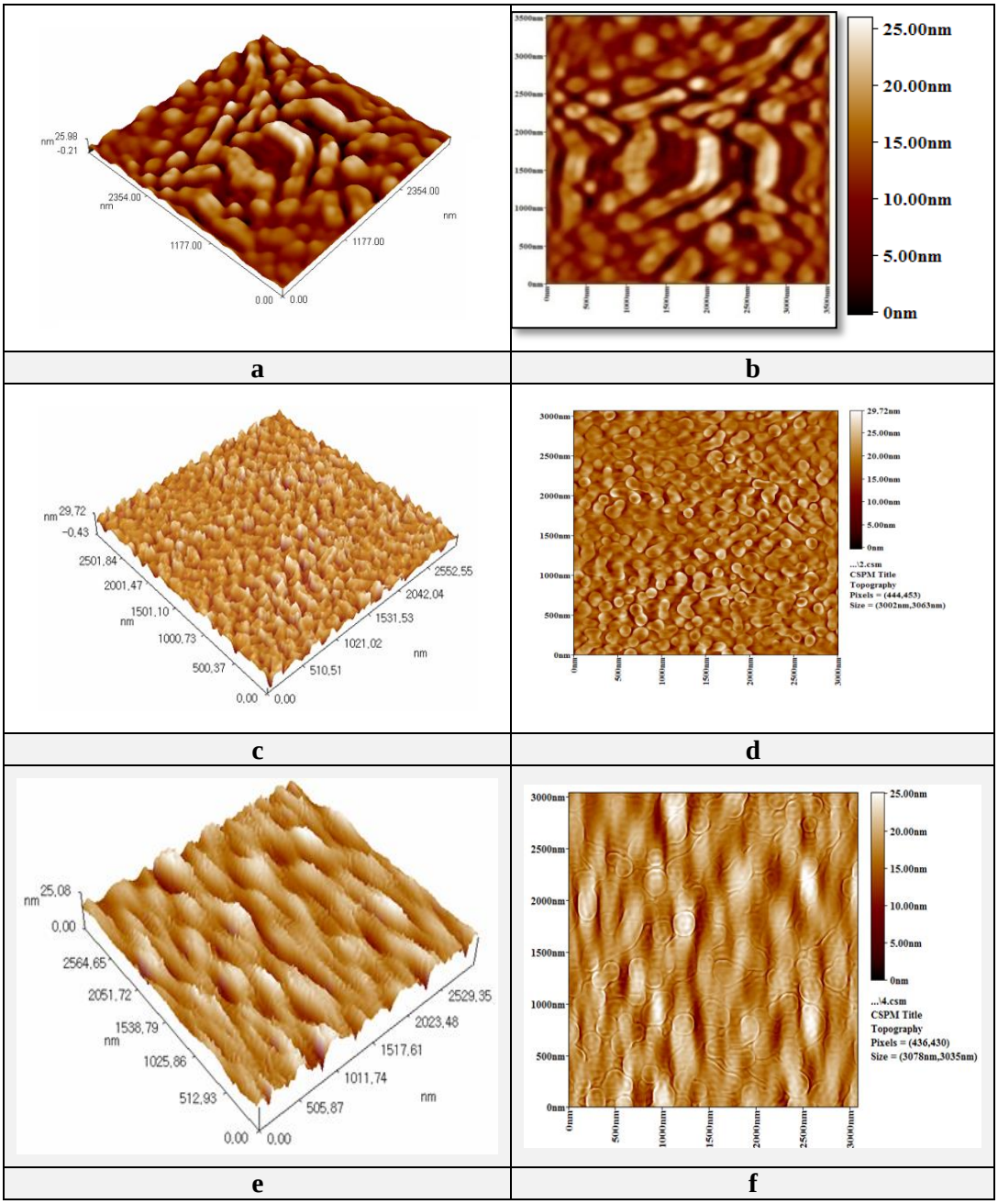

Figure 17- AFM image of carbon steel surface. (a, b); in a 3.5% NaCl saline solutions, (c, d); in presence of 20 ppm of (IMID4) inhibitor, and (e,f) in presence of 20 ppm of (OXAZ5) inhibitor.

Conclusions

1. The newly synthesized inhibitors (IMID4 and OXAZ5) were theoretically found to be good organic corrosion inhibitors for carbon steel in saline water with an order of inhibition efficiencies (%IE) of: IMID4 (89.093%) > OXAZ5 (80.179%).
2. The inhibition efficiency was measured for inhibitors using potentiodynamic polarization measurements indicated that the studied inhibitors are classified as mixed inhibitors in saline water, because the addition of the two inhibitors is found to affect both the anodic and cathodic process.
3. The inhibition efficiency increased with the increase of inhibitors concentration and decreased with the increase of temperature (physisorption inhibition).
4. The adsorption of the studied compounds on carbon steel surface followed the Langmuir adsorption isotherm model. The high values of the equilibrium constant which obtained from the Langmuir isotherm for both inhibitors indicates stronger adsorption on the carbon steel surface in 3.5% NaCl

solution. The negative value of (ΔG^0_{ads}) indicates that the adsorption of (IMID4 and OXAZ5) on mild steel surface is a spontaneous process.
5- SEM and AFM images have shown that inhibition of corrosion by (IMID4 and OXAZ5) inhibitors is due to the formation of a physisorbed film on the metal surface.

References

1. Fan, Z. **2013**. "The Mussel Adhesive Protein (Mefp-1)- A Green Corrosion Inhibitor". Ph.D Thesis Stockholm, Sweden.
2. Kubba, R.M., Challoob, D.A and Hussen, S.M. **2017**. Quantum mechanical and electrochemical study of new isatin derivative as corrosion inhibitor for carbon steel in 3.5 % NaCl. *Int. J. of Sci. and Res*, **6**(7): 1656-1669.
3. Abdallah, M., Asghar, B.H., Zaafarany, I. and Fouda, A.S. **2012**. The inhibition of carbon steel corrosion in hydrochloric acid solution using some phenolic compounds, *Int. J. Electrochem. Sci*., (7): 282-304.
4. Ahmed, A.H., Kubba R.M. and Al-Majidi S.M.H. **2018**. Synthesis, identification, theoretical and experimental studies of carbon steel corrosion inhibition in sea water by some new diazine derivatives linked to 5-nitro isatin moiety. *Iraqi Journal of Science*, **59**(3B): 1347-1365.
5. Fouda , A.S., Abd El-Maksoud, S.A., El-Hossiany, A. and Ibrahim, A. **2019**. Corrosion protection of stainless steel 201 in acidic media using novel hydrazine derivatives as corrosion inhibitors. *Int. J. Electrochem. Sci*., (14): 2187 – 2207
6. Obot, I.B., Macdonald, D.D. and Gasem, Z.M. **2015**. Density Functional Theory (DFT) as a powerful tool for designing new organic corrosion inhibitors. Part 1: An overview. *Corrosion* Science, **99**: 1-30.
7. Shaban SM. **2016**. N-(3-(dimethyl benzyl ammonium) propyl) alkanamide chloride derivatives as corrosion inhibitors for mild steel in 1 M HCl solution: Experimental and theoretical investigation. *RSC Advances*, (6): 39784-39800
8. Al-Lami, N. and Salom K.J. **2018**. Synthesis and biological activity evaluation of new imidazo and bis imidazo (1,2-A) pyridine derivatives. *J. Glob. Pharm. Tech*., **10**(11): 603-611.
9. Duboscq, J., Sabot, R., Jeannin M. and Refait, Ph. **2019**. Localized corrosion of carbon steel in seawater: Processes occurring in cathodic zones. *Materials and corrosion*.m **70**(6): 973-984.
10. Rajendran, M., Keerthika, K., Kowsalya, M. and Devapiriam, D. **2016**. Theoretical studies on corrosion inhibition efficiency of pyridine carbonyl derivatives using DFT method. *Der. Pharma. Chemica.*, **8**(3): 1-79.
11. Becke, A. **1993**. Density-functional thermochemistry. III. The role of exact exchange. *Journal of Chem. and Phys.* **98**: 5648-5652.
12. Kubba R.M. and Mohammed, M. **2016**. Theoretical studies of corrosion inhibition efficiency of two new N-phenyl-ethylidene-5-bromo isatin derivatives. *Iraqi Journal of Science*, **57**(2B): 1041-1051.
13. Zhang, J., Liu, J., Yu, W., Yan, Y., You, L. and Liu, L. **2010**. Molecular modeling of the inhibition mechanism of 1- (2-aminoethyl)-2-alkyl-imidazoline, *Corros. Sci*., **52**(6): 2059-2065.
14. Tafel, J. Polarization in cathodic hydrogen evolution, **1905.** *Zeitschrift Fuer Physikalische Chemie,Stoechiometrie and Verwandtschaftslehre*, **50**: 641-712.
15. Hong, S., Chen, W., Luo, H.Q. and Li, N.B. **2012**. Inhibition effect of 4-amino-antipyrine on the corrosion of copper in 3 wt. % NaCl solution, *Corro. Sci*., **57**: 270–278.
16. Ben Hmamou, D., -Aouad, M., Salghi, R., Zarrouk, A., Assouag, M., Benali, O., Messali, M., Zarrok, H. and Hammouti, B. **2012**. Inhibition of C38 steel corrosion in hydrochloric acid solution by 4,5- diphenyl-1H-imidazole-2-thiol:gravimetric and temperature effects treatments. *Int. J. of Sci. and Res*. **4**(7): 3498-3504.
17. Abd-El-Naby, B., Abdullatef, O., Khamis, E. and El-Mahmody, W. **2016**. Effect of cetyl trimethyl ammonium bromide surfactant as novel inhibitor for the corrosion of steel in 0.5 M H_2SO_4. *Int.J. Electrochem.and Sci*. **11**: 1271-1281.
18. Singh, A., Ansari, K.R., Lin, Y., Quraishi, M.A., Lgaz, H. and Ill-Min Chung. **2018**. Corrosion inhibition performance of imidazolidine derivatives for J55 pipeline steel in acidic oilfield formation water: Electrochemical, surface and theoretical studies. *J. of Taiw. Inst. of Chem. Eng.*, 0 0 0, 1–16

19. Louadi, Y.E., Abrigach, F., Bouyanzer, A., Touzani, R., El Assyry, A., Zarrouk, A., and Hammoutia, B. **2017**. Theoretical and Experimental Studies on the Corrosion Inhibition Potentials of Two Tetrakis Pyrazole Derivatives for Mild Steel in 1.0M HCl. *Portugaliae Electrochimica Acta*, **35(**3): 159-178.

20. Mohamed, A., Khaled, Z., Hamdy, A., Abo-Elenien, O. and Olfat, E. **2015**. Synthesis of novel schiff base silicon compound for employing as corrosion inhibitor for carbon steel in the 1 M HCL and 3.5% NaCl aqueous media. *International Journal of Chemical, Environmental & Biological Sciences*, **3**: 2320-4087.

21. Gowri, S., Sathiyabama, J., Prabhakar, P. and Rajendran, S. **2012**. Inhibition behaviour of carbon steel in sea water in the presence of tyrosine- Zn^{2+} system. *International Journal of Research in Chemistry and Environment*, **3**: 156-162.